Carbon 95 (2015) 292–301

Contents lists available at ScienceDirect

Carbon

journal homepage: www.elsevier.com/locate/carbon

Rational recipe for bulk growth of graphene/carbon nanotube hybrids: New insights from *in-situ* characterization on working catalysts

Tian-Chi Chen, Qiang Zhang*, Meng-Qiang Zhao, Jia-Qi Huang, Cheng Tang, Fei Wei

Beijing Key Laboratory of Green Chemical Reaction Engineering and Technology, Department of Chemical Engineering, Tsinghua University, Beijing 100084, China

ARTICLE INFO

Article history:
Received 30 April 2015
Received in revised form
11 August 2015
Accepted 15 August 2015
Available online 17 August 2015

ABSTRACT

The graphene/carbon nanotube (CNT) hybrids are considered as one of the most advanced nanostructures with intrinsically self-dispersion properties for large-volume applications. However, owing to the limited understanding on the complex growth mechanism and non-linear kinetics, rational design of growth procedures and related multiphase reactors for the production of the hybrids remain great challenges. In this contribution, the *in-situ* monitoring of graphene/CNT hybrid synthesis on layered double oxide bifunctional catalysts was carried out in an online thermogravimetric reactor. The rapid growth of CNTs occurred at the initial 90 s and the slow deposition of graphene was throughout the whole process, becoming the dominant reaction in the second stage. Based on this unique growth behavior, a two-stage growth strategy was proposed to improve the quality of hybrid products. The deposition of amorphous carbon byproduct was significantly suppressed and the quality of the hybrids was significantly enhanced through the two-stage growth process.

1. Introduction

The ubiquitous carbon-based nanomaterials, including zero-dimensional (0D) fullerene, one-dimensional (1D) carbon nanotubes (CNTs), two-dimensional (2D) graphene and other related nanocarbons, have attracted tremendous attention owing to their extraordinary electrical and mechanical properties for a broad field of potential applications [1,2]. However, both 1D CNTs and 2D graphene are inclined to aggregate or stack with each other due to the strong van der Waals forces, which hinder the full exposure of active interfaces for the applications in energy storage and gas sorption [2]. If the 1D CNTs and 2D graphene are rationally integrated into three dimensional (3D) graphene/CNT hybrids, not only the virtues of both graphene and CNTs are inherited, but also effective electronic and thermal conductive 3D networks with an intrinsic dispersion are obtained. Such advanced 3D nanostructures afford unique mechanical, electrical and thermal properties and superior performance in energy storage [3–11], electronic devices [12–14], as well as chemical conversion [12,15,16].

Up to now, myriad approaches have been developed to fabricate this hybrid 3D structure [17], among which the post-synthesis methods were initially explored. Routes including directing mixing [18,19], liquid phase reactions [11,12], casting processes [20], layer-by-layer self-assembly [21–23], evaporation at liquid–air interface [24], hydrothermal fabrication [9,25], electrophoretic deposition [26], and vacuum-assisted filtration [10] have been demonstrated successfully. However, they cannot provide effective connections (*e.g.* the covalent C–C bonding) between graphene and CNTs. This strongly hinders the quality of the products and their further applications. On the contrary, the direct growth method through chemical vapor deposition (CVD) exhibits its advantages in providing the possibility to form the C–C covalent bonding and the variety of anticipated structures [5,8,13,27–31]. Thus, growing CNTs on graphene layers [5,13,14,27–32] and the *in-situ* growth of the hybrids on Cu foil coated with Fe catalyst layers [7,32] were successively reported.

Although these methods are simple and effective to obtain strong graphene-CNT bonding, the growth of CNTs and graphene are quite complex and asynchronous on the bifunctional catalysts [33,34]. In most cases, CNTs preferred to grow on metal catalyst nanoparticles (NPs) and graphene was inclined to deposit on the surface of Cu or metal oxide. Both the bifunctional catalysts and related reactor technologies were highly required for efficient bulk growth of graphene/CNT hybrids. Due to the limited understanding of the growth behavior of hybrids on the bifunctional catalysts, the recipe for large scale production is few touched, although this is the

* Corresponding author.
E-mail address: zhang-qiang@mails.tsinghua.edu.cn (Q. Zhang).

http://dx.doi.org/10.1016/j.carbon.2015.08.044
0008-6223/

first and core step to obtain high quality hybrid samples for the exploration on their bulk application.

In this contribution, the working bifunctional catalyst for graphene/single-walled CNT hybrids (GSHs) was *in-situ* monitored in a thermogravimetric (TG) reactor. The reason to select graphene and single-walled CNTs as the building blocks was attributed from their ubiquitous properties, potentials for bulk applications in high-end products, and their notorious difficulty in good dispersion of each building block. GSHs were widely accepted as the high-end nanocarbon materials for bulk applications in energy storage, adsorption, environmental protection, as well as multifunctional composites [3,4,12,13]. Herein, the growth mechanism of GSH on bifunctional layered double oxide (LDO) catalysts was probed to distinguish the growth rate and duration among CNTs, graphene, and the impurities of amorphous carbon. Based on the growth behavior recorded by the *in-situ* characterization, a two-stage growth strategy was proposed to improve the process efficiency and GSH product quality. Compared with the GSHs fabricated in the routine one-stage way, the GSHs grown in the two-stage method presented a higher purity with fewer amorphous carbons and a larger surface area for their potential applications in energy storage and other fields.

2. Experimental

2.1. Catalyst preparation

The FeMgAl layered double hydroxides (LDHs) were prepared using a facile urea-assisted co-precipitation reaction. Typically, $Fe(NO_3)_3\cdot 6H_2O$, $Mg(NO_3)_2\cdot 6H_2O$, $Al(NO_3)_3\cdot 9H_2O$, and urea were dissolved in 2000 mL deionized water with [urea] = 3.0 mol L^{-1}, n(Fe):n(Mg):n(Al) = 0.4:3:1, and $[Fe^{3+}] + [Mg^{2+}] + [Al^{3+}] = 0.15$ mol L^{-1}. The mixture was then transferred to a 5000 mL glass flask equipped with a reflux condenser. The solution was kept at 100 °C under continuous magnetic stirring for 12.0 h and maintained at 94 °C for 12.0 h without stirring. The FeMgAl LDHs were finally obtained after filtering the as-obtained suspension, washing, and freeze-drying. The $[Mg_{0.69}Al_{0.23}Fe_{0.08}(OH)_2][(CO_3)_{0.155}]\cdot mH_2O$ LDHs were calcined at 900 °C for 0.5 h to obtain FeMgAl layered double oxide (LDO) bifunctional catalysts for GSH growth.

2.2. In-situ monitoring the GSH growth in the TG reactor

In-situ TG investigation of the GSH growth was operated in a TGA/DSC1 STAR^e system. As shown in Fig. 1, 2.0 mg FeMgAl LDO flakes were put into a 70 μL Al_2O_3 crucible, which was inserted into the furnace of the TGA/DSC1 STAR^e system. Then, the furnace was heated to 950 °C with a heating rate of 20 °C min^{-1} under Ar (100 mL min^{-1}) atmosphere. On reaching the reaction temperature, the Ar was switched to the gas mixture of CH_4/Ar with a flow rate of 80/20 mL min^{-1} to start the growth of GSHs. The GSH growth reaction was maintained for 30 min. The mass of working catalysts was recorded by the online mass balance attached with the TG reactor, the reaction heat was *in-situ* collected as the balanced voltage in this system, and the feedstock conversion was determined by the attached on-line mass spectroscopy.

2.3. Bulk growth of GSHs

Bulk CVD growth was carried out to obtain the GSHs on FeMgAl bifunctional LDO catalysts both in a routine way and the coupled two-stage method. A quartz fluidized bed reactor with an inner diameter of 50 mm and a height of 1500 mm was employed. There was a porous sintered quartz plate distributor at the middle of the fluidized bed reactor that served as the support for LDO catalysts and products at the same time. The up-flowing gas mixture entered the reactor from the bottom and then passed through the gas distributor, the fluidized bed unit, and then flowed out from the top of the reactor. During the routine fluidized bed CVD, 10.0 g Fe/Mg/Al LDO catalysts were uniformly fed into the reactor, which was then inserted into a vertical electric tube furnace and heated to 950 °C under Ar atmosphere. The apparent gas velocity was 0.1 m s^{-1} and the methane feed rate was 0.05 g_{CH4} g_{LDO}^{-1} min^{-1}. The growth duration is 15 min. The as-grown samples on the LDO flakes were denoted as one-stage GSHs. While in the two-stage growth procedure, 10.0 g Fe/Mg/Al LDO catalysts were firstly fed into a fluidized bed reactor. CH_4 with a feed rate of 0.15 g_{CH4} g_{LDO}^{-1} min^{-1} was introduced for 90 s as the first growth period. Then the feed rate of the carbon sources was turned down to 0.03 g_{CH4} g_{LDO}^{-1} min^{-1} for another 810 s at 950 °C. After that, the fluidized bed reactor was cooled down to room temperature under Ar protection. The as-obtained products were the two-stage GSHs grown on FeMgAl LDO bifunctional catalysts.

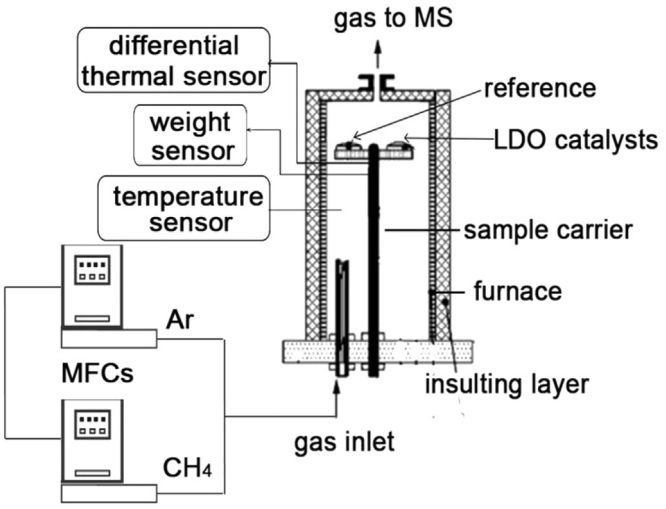

Fig. 1. Schematic illustration of the online TG reactor.

The as-grown raw GSH products were purified with a combined alkali and acid treatment to remove the FeMgAl LDO flakes. Typically, the samples were firstly hydrothermally treated by NaOH solution (15.0 mol L^{-1}) at a temperature of 150 °C for 12.0 h. Subsequently, the as-obtained products were then immersed into HCl solution (3.0 mol L^{-1}) at a temperature of 80 °C for 12.0 h. The as-obtained products were then filtered, washed by deionized water, and freeze-drying, leaving the purified GSH samples (denoted as two-stage GSHs and one-stage GSHs, respectively).

2.4. Characterizations

The morphology of the LDO flakes and the as-grown products were characterized by a JSM 7401F (JEOL Ltd., Tokyo, Japan) scanning electron microscopy (SEM) operated at 3.0 kV, a JEM 2010 (JEOL Ltd, Tokyo, Japan) TEM operated at 120.0 kV and a spherical aberration-corrected Titan3 60–300 (FEI Company) microscope operated at 80.0 kV. The thermogravimetric analysis (TGA) under CO_2 atmosphere was performed using a Mettler Toledo TGA/DSC-1 analyzer. Typically, about 5.0 mg samples were laid into a 70 μL Al_2O_3 crucible, which was inserted into the furnace of the TGA/DSC1 STAR^e system. Then the furnace was heated from 30 to 1400 °C with a heating rate of 20 °C min^{-1} under a mixture of N_2/CO_2 (50/50 mL min^{-1}) atmosphere. The Raman spectra were

collected with a He–Ne laser excited at 633 nm using Horiba Jobin Yvon LabRAM HR800 Raman Spectrometer. The pore volume, size distribution, and Brunauer–Emmett–Teller (BET) specific surface area (SSA) of the samples were calculated from the N_2 adsorption–desorption isotherms measured by Autosorb-IQ_2-MP-C system. Before the measurement, samples were degassed at 300 °C until a manifold pressure of 2.0 mmHg was reached. A four-probe method was performed to detect the powder conductivity of the GSHs, which were compressed into a dense disk with 13.0 mm-diameter under a pressure of 8.0 MPa.

3. Results and discussion

3.1. In-situ TG investigation of the growth of GSHs

LDHs, which are a kind of hydrotalcite-like material composed of positively-charged layers and charge-balancing interlayer anions [35], can afford continuous flat metal oxide substrate *via* facile calcination as a hard template for the CVD growth of graphene [36]. The resulting LDOs can be reduced to generate embedded high-density small-sized catalyst nanoparticles (<5 nm) with extraordinary thermal stability [37]. These tiny metal nanoparticles are effective for catalytic deposition of CNTs.

As illustrated in Fig. 2, the FeMgAl LDO flakes were used as the bifunctional catalysts for the high-temperature CVD growth of GSHs. The *in-situ* reduced Fe NPs embedded on the LDO flakes were served as the catalysts for single-walled CNT growth, while the 2D lamellar metal oxide substrates were employed as the template for graphene deposition. High purity GSHs were obtained after the removal of LDO flakes through chemical treatment of the as-grown products.

To probe the kinetics on the working LDO catalyst for GSH growth, *in-situ* TG investigation was carried out. The TG and differential TG (DTG) profiles of GSH formation with a growth duration of 30 min were presented as Fig. 3a. The increasing rate of sample weight was recorded as the growth rate of GSHs. An obvious two-stage growth was observed, including a rapid reaction procedure with a large growth rate of GSHs at initial 90 s, and a slow growth process with a tiny gradual rise after that. The largest growth rate of 0.013 $g_C\ g_{cat}^{-1}\ s^{-1}$ at around 40 s was achieved. The average rate of mass increase was about 0.009 $g_C\ g_{cat}^{-1}\ s^{-1}$ in the first stage (0–90 s), but only 0.003 $g_C\ g_{cat}^{-1}\ s^{-1}$ for the subsequent reaction in the second stage.

The differential thermal analysis (DTA) profile of the GSH growth illustrated a sharp endothermic peak in the first stage (0–90 s) while no obvious reaction heat was detected during the following period (Fig. 3b). A higher conversion for the first stage than the second stage is inferred from the DTA plot since the decomposition of methane was an endothermic reaction. Such trend consisted with the above-mentioned two-stage growth behavior of GSHs based on TGA data, from which the average methane conversion of the first stage could be roughly estimated as 2.5% while the value for the second stage was less than 1.0%.

The attached on-line mass spectrometer collected the real-time gaseous reactant and product concentration during GSH growth (Fig. 3c). The initial starting point was set as the introduction of CH_4 to the LDO catalysts. Besides methane and hydrogen, many kinds of hydrocarbons (such as ethane, ethylene, propane, as well as propylene) were also detected, indicating the synthesis of GSHs was complex coupling reactions involving a variety of carbon species. The thermal conversion of CH_4 into other hydrocarbons, which is thermodynamically derived from C–H bonding activation and hydrocarbon transformation has been highly concerned during the ethylene production and pyrolytic carbon deposition [38]. Herein, FeMgAl LDO flakes were employed as the bifunctional catalysts for GSH formation. The formation mechanism of the other hydrocarbons was assumed as:

$$2\ CH_4 \leftrightarrow C_2H_6 + H_2 \quad (1)$$

$$C_2H_6 \leftrightarrow C_2H_4 + H_2 \quad (2)$$

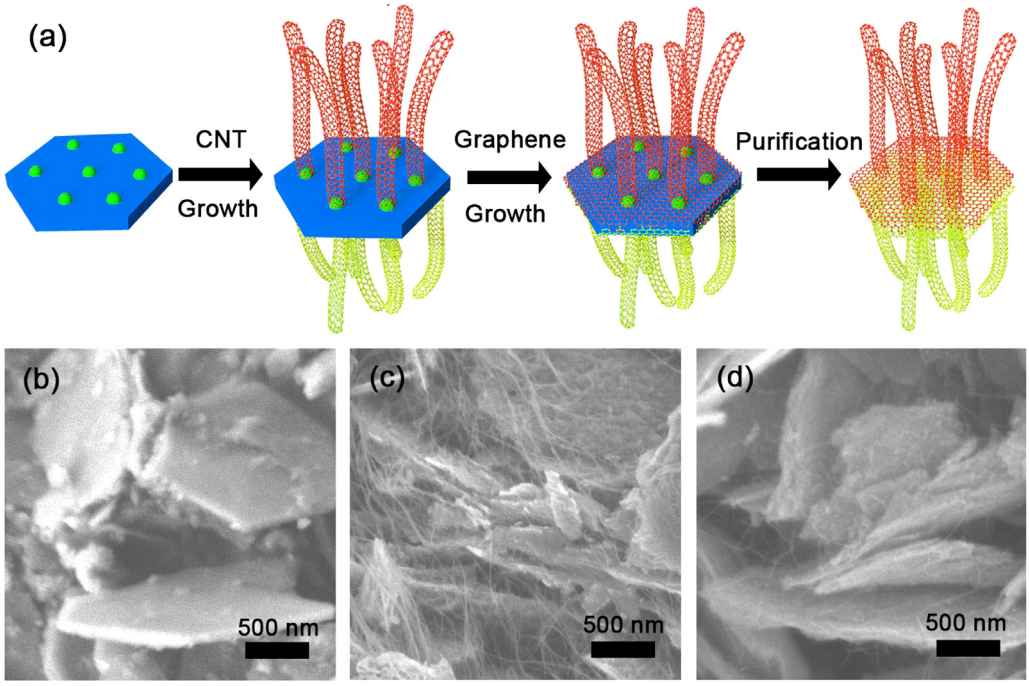

Fig. 2. Growth of GSHs on bifunctional catalysts. (a) Schematic illustration of CVD growth of GSHs on LDO flakes. SEM images of (b) bifunctional LDO catalysts, (c) GSH-LDO products, and (d) purified GSHs after removing catalysts. (A colour version of this figure can be viewed online.)

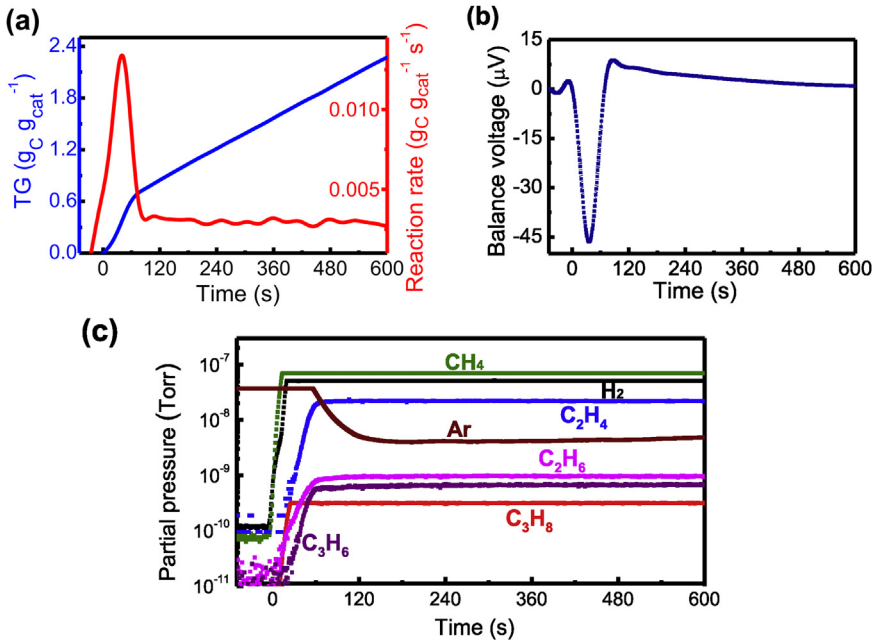

Fig. 3. *In-situ* growth of GSHs on working bifunctional LDO catalysts. (a) TG and DTG profiles of GSH products during CVD in a TG reactor; (b) DTA profile of the CVD growth; (c) MS profiles of the gaseous reactants and products extracted from the TG reactor. (A colour version of this figure can be viewed online.)

$$C_2H_4 + CH_4 \leftrightarrow C_3H_8 \quad (3)$$

$$C_3H_8 \leftrightarrow C_3H_6 + H_2 \quad (4)$$

As illustrated in Fig. 3c, the concentrations of ethane, propane, and propylene were very low, while the ethylene concentration was high during the whole growth duration. Similar to the TG and DTA profiles, the concentration changes of these gas products also exhibited a two-stage procedure. During the first stage of rapid single-walled CNT and few-layer graphene formation, the methane was in high conversion, while few amounts of ethane, ethylene, propane, and propylene were detected. With the rapid formation of single-walled CNTs and gradually deactivation of metal NPs, the conversion of methane became low, while the amount of propane increase sharply between 15 and 25 s. The amount of ethane, ethylene, and propylene rise during 20–50 s. It should be noticed that the ethylene concentration is two orders of magnitude higher than those of ethane, propane, and propylene, but still is one-fifth of the value for methane at a temperature of 950 °C during the second stage of graphene deposition. It is widely accepted that the addition of ethylene into methane enhances the CNT formation, and C_2 is believed to be the most active carbon precursors for single-walled CNT formation [39]. While for graphene deposition, the methane is favorable to be cracked into carbon atom and hydrogen on the exposed oxygen of the metal oxide templates, while thermal cracking products of ethylene are well preserved. The carbon deposition routes for single-walled CNTs and graphene formation are quite different and not fully understood yet. At least we can conclude that a two-stage growth of GSHs is unambiguously confirmed by the *in-situ* TG analysis.

Recently, *in-situ* Raman spectroscopy [40–42], *in-situ* scanning electron microscope (SEM) [43], *in-situ* transmission electron microscope (TEM) [44], *in-situ* X-ray photoelectron spectroscopy [45], *in-situ* thermogravimetric analysis [46–48] have been employed to probe the formation of CNTs or graphene. These results provide direct evidences to reveal the complex reaction pathways and afford insightful principle for nanocarbon formation. However, few information on the complex kinetics of nanocarbon formation is revealed and kinetic modeling is highly required [49]. This contribution is the first report to monitor the working bifunctional catalysts for the 3D hybrid carbon formation. The working behavior of both metal nanoparticles and metal oxide substrates was *in-situ* probed, and the nanostructures of the raw products were further probed by TEM and Raman spectroscopy to further correlate the structure of GSHs and working behavior of LDO catalysts.

The GSH samples with growth durations of 1.5, 10, and 30 min, denoted as GSH-1.5, GSH-10, and GSH-30 according to their growth duration, respectively, were collected and characterized by both Raman spectroscopy and TEM. The Raman spectra (Fig. 4a) revealed that the value of I_G/I_D ratio of GSH-1.5, GSH-10, and GSH-30 were 7.4, 2.0, and 1.2, respectively. This indicated a significant degrading for the graphitization of the as-obtained GSHs with a long growth duration. Besides, the signal-to-noise ratio of the radial breathing mode (RBM) peaks between 100 and 300 cm^{-1} on the Raman spectra (Fig. 4b), which represented the existence of single-walled CNTs, also significantly decreased along with the extending growth duration. A negative trend for the ratio of single-walled CNTs in the GSHs was demonstrated. The TEM images of the corresponding samples were presented in Fig. 4c–e. It can be noticed that the predominant products of GSH-1.5 were single-walled CNTs (Fig. 4c), while an increase of graphene amount with few amorphous carbon was observed in GSH-10 (Fig. 4d) compared to GSH-1.5.

Fig. 4f presented the graphene region in the sample of GSH-10. This indicated GSHs were mainly composed of few-layer graphene (<5 layers) along with single-walled CNTs. When further extending the growth duration to 30 min (GSH-30), both the thickness of the graphene and the amount of amorphous carbon significantly increased (Fig. 4e). This was in good agreement with the expectation based on the above-mentioned Raman spectra shown as Fig. 4a and b.

Combined with the trends reflected by the results collected during the *in-situ* growth in a TG analyzer, it came to the deduction that the mass increase observed during the initial 90 s was mainly

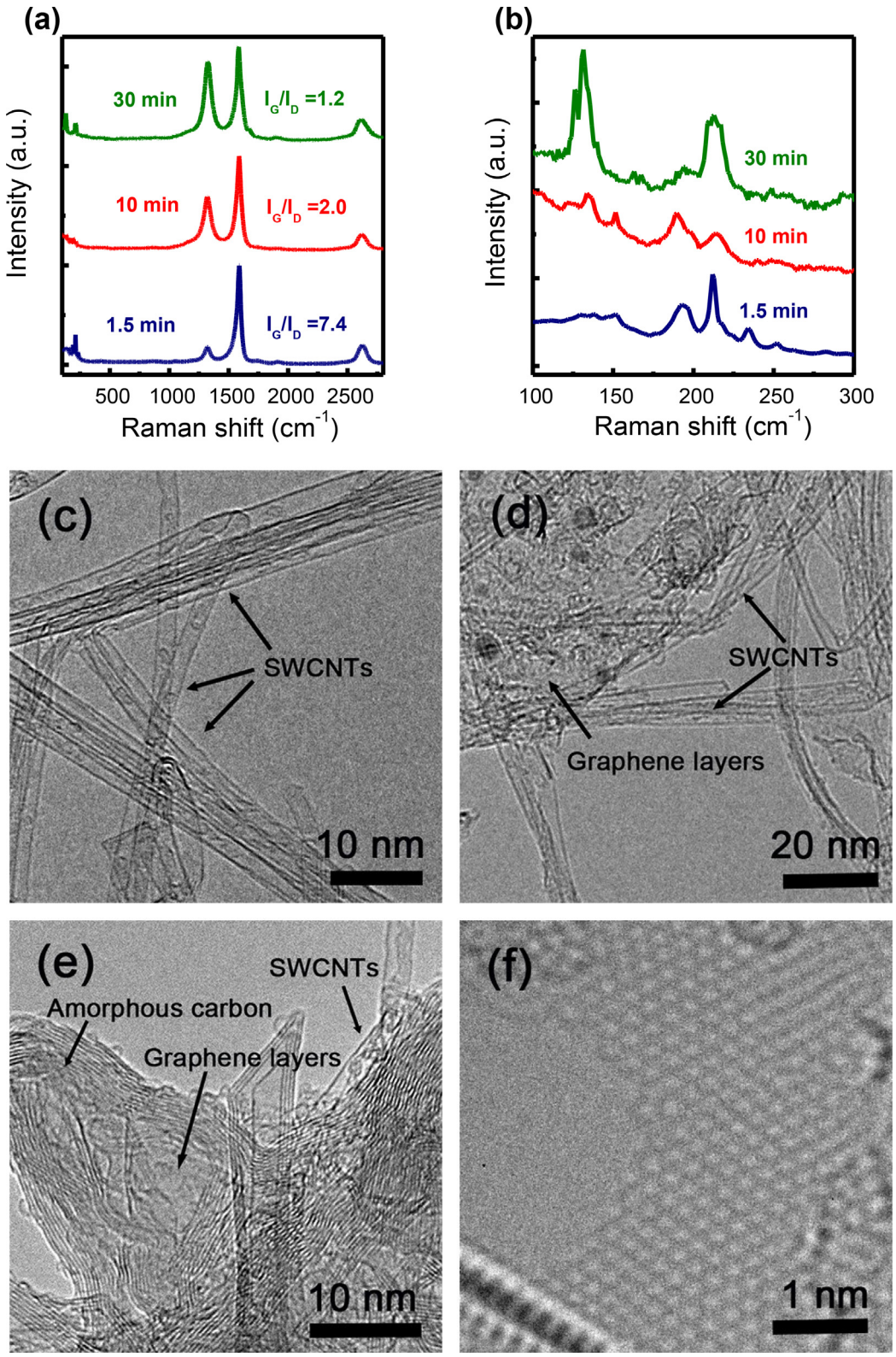

Fig. 4. Characterization of GSHs with different growth durations. (a) Raman spectra of three GSH samples; (b) Corresponding RBM peaks in Raman spectra. TEM images of GSHs grown for (c) 1.5 min, (d) 10 min, and (e) 30 min. (f) High-resolution TEM image of the corresponding domain of the 10 min-GSH sample, showing the existence of few-layer graphene. (A colour version of this figure can be viewed online.)

corresponding to the formation of single-walled CNTs, along with the deposition of some few-layer graphene. The Fe nanoparticles in the bifunctional LDO catalysts were deactivated after the rapid growth of CNTs with an average growth rate of 0.009 $g_C\ g_{cat}^{-1}\ s^{-1}$. The following 1710 s reaction was accounted for the continual deposition of graphene layers and amorphous carbon with an average graphene growth rate of only 0.003 $g_C\ g_{cat}^{-1}\ s^{-1}$. This growth rate was around one third of the first period.

3.2. Rational recipe for the bulk growth of GSHs

Rational design of growth procedures and related multiphase reactors for bulk production of GSHs is the first step for their large volume applications. The fluidized bed reactor has been regarded as the most commonly used apparatus for the mass production of carbon nanomaterials [50–53]. Efficient bulk growth of multi-walled CNTs [50–53], single-walled CNTs [54,55], aligned CNTs [56–59], and graphene [36] have been successfully achieved through a catalytic fluidized bed CVD. Recently, we reported controllable mass production of GSHs in a fluidized bed reactor [60]. The GSHs were fabricated on the FeMgAl LDO flakes serving as bifunctional catalysts due to their good fluidization behavior [55]. The yield and quality of the as-grown products can be well modulated by adjusting the Fe content in LDH precursors. However, considering the unique two-stage growth features of the GSHs revealed by the *in-situ* TG analysis, the one-step procedure in a fluidized bed reactor alone still suffered from several technical problems. For instance, the flow rate of carbon source was too high in the second-stage of graphene formation. The rapid CNT formation had been terminated and the carbon deposition rate decreased to only about one-third of the value for the first stage during the second period. If the methane flow rate remained constant as in a routine one-step growth, the extra part of carbon sources would not only induce unnecessary consumptions of materials and energy, but also probably lead to the formation of large amount of amorphous carbon by-products. The graphene sheets became thicker and amorphous carbon was attached onto the outer surface of CNTs and graphene, which significantly degraded the quality of GSH products and hindered their intrinsic properties [61].

Therefore, a two-stage growth strategy was proposed for the bulk growth of GSHs herein. Firstly, the catalysts carried by the gases (mixture of Ar and CH_4) were fed into a fluidized bed reactor operated at 950 °C. The residence time of catalysts was controlled to be less than 90 s and a relatively high methane feed rate of 0.15 g_{CH4} g_{LDO}^{-1} min^{-1} was employed for the rapid growth of the first stage, attributing mainly from the single-walled CNTs. After that, the methane feed rate decreased to 0.03 g_{CH4} g_{LDO}^{-1} min^{-1}, in which graphene were the dominant products. Such two-stage growth can be even realized in a proposed coupled fluidized bed reactor shown in Fig. 5b.

Firstly, the single-walled CNTs were rapidly formed on metal nanoparticles embedded on the LDO catalysts at a low temperature of 850–900 °C with a high feed rate of carbon sources, while few graphene/amorphous carbon was deposited yet. Then CNT-LDO products were transferred into the next fluidized bed for continual graphene growth on the oxides with a low feed rate of carbon sources at 950 °C. Such delicate system was beneficial for effective GSH formation with controllable growth atmosphere. It was expected that higher-quality GSHs with an increased ratio of single-walled CNTs and single-layer graphene could be fabricated with this reaction technology than the previously reported one-stage fluidized bed.

3.3. Two-stage synthesis of GSHs

In order to verify the feasibility and superiority of the proposed two-stage method, a high-temperature two-stage CVD for GSH growth in a single fluidized bed reactor was adopted. The products were denoted as two-stage GSHs. In contrast, the GSH sample produced *via* a routine way was applied as a control sample, denoted as one-stage GSHs. SEM and TEM images illustrated the typical morphology of the as-obtained two-stage and one-stage GSHs (Fig. 6). Large amount of single-walled CNTs and graphene were demonstrated on the surface of the FeMgAl LDO flakes in both of the samples (Fig. 6a, b). Compared to the one-stage GSHs (Fig. 6c, d), the two-stage GSHs (Fig. 6e, f) exhibited a much higher proportion of few-layer graphene instead of multilayer graphene and a significantly smaller amount of amorphous carbon. The spherical aberration-corrected high-resolution TEM image of few-layer graphene domain of two-stage GSHs were presented as Fig. 6g. To discuss if single-walled CNTs and graphene had covalent C–C bonding at the interfaces, further delicate characterization is highly required.

TGA test under CO_2 atmosphere was carried out to characterize the mass ratio of single-walled CNTs, graphene, and amorphous carbon in the GSHs. It has been well proven that the first weight loss region accounts for the oxidation of impurities (including amorphous carbon) and part of the graphene materials, and the second weight loss region mainly corresponds to the oxidation of single-walled CNTs [6]. As shown in Fig. 7a, a weight loss of 34.3 and 65.7% of the two-stage GSHs was observed during the first and second region, respectively, while the value for the one-stage GSHs was 70.8 and 29.2%. The two-stage GSHs presented an improved thermal stability and a higher ratio of CNT components in the hybrid products, which were in good agreement with the observation based on SEM and TEM images.

There were large quantities of single-walled CNTs in both GSH samples, which were confirmed by the obvious RBM peaks between 100 and 300 cm^{-1} on the Raman spectra shown as Fig. 7b. The I_G/I_D ratio was increased from 1.2 of one-stage GSHs to 1.6 of two-stage GSHs, revealing the improvement in the degree of

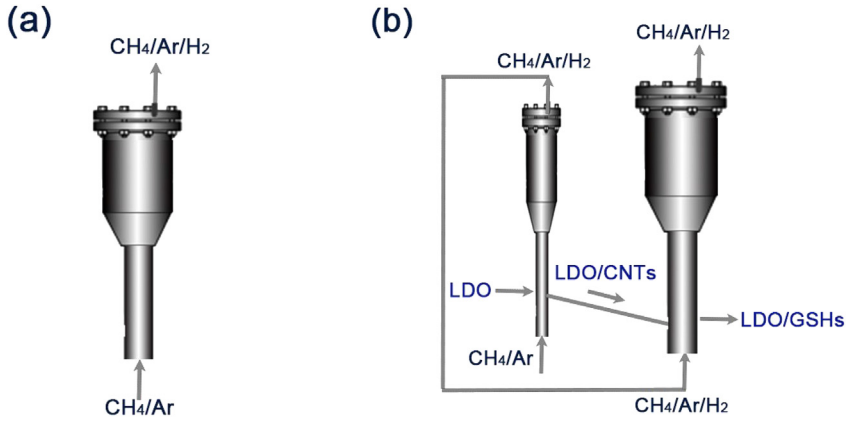

Fig. 5. Schematic illustration of (a) the current used single fluidized bed reactor (b) the proposed coupled two-stage fluidized bed reactor system for efficient growth of GSHs. (A colour version of this figure can be viewed online.)

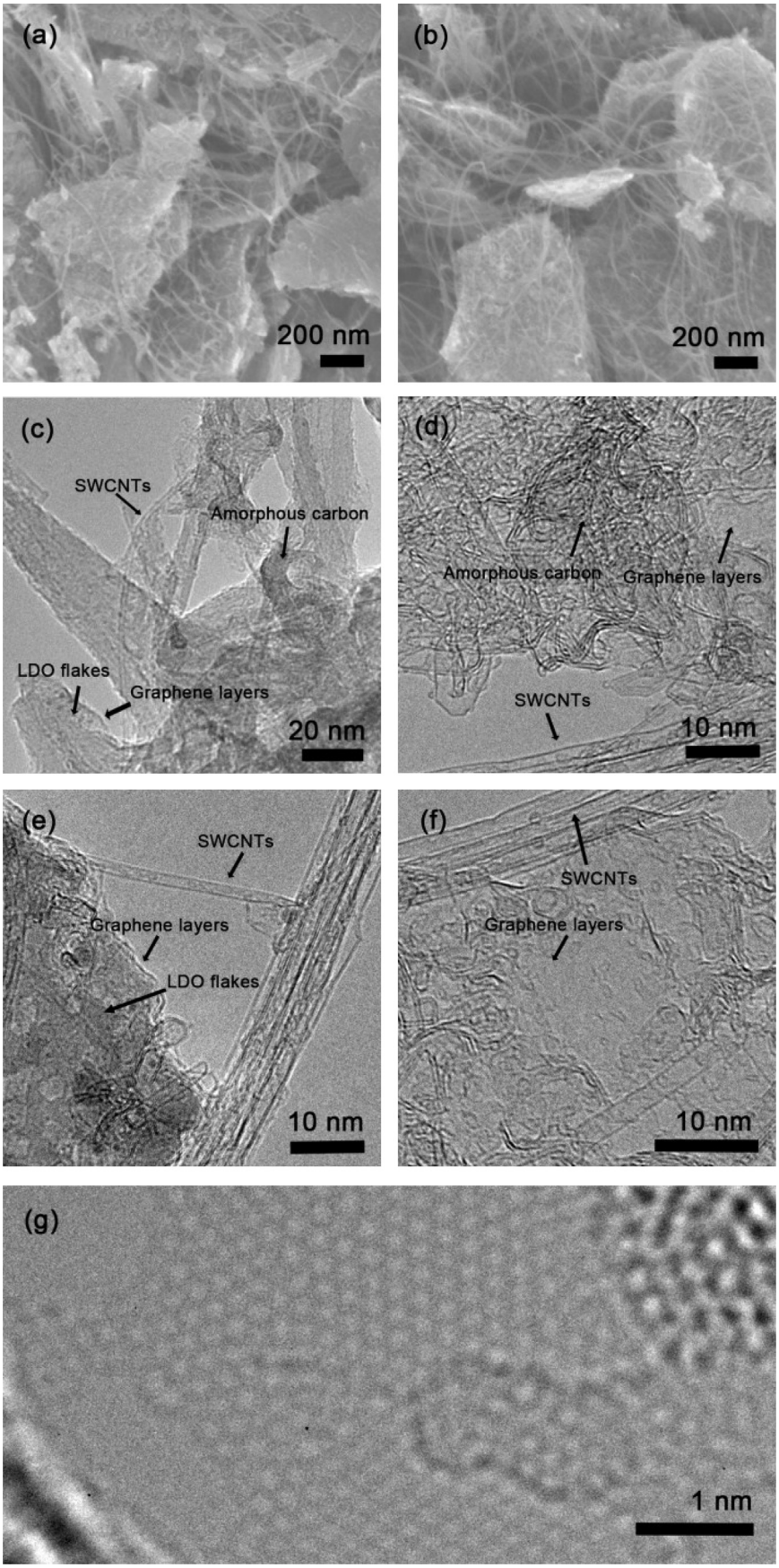

Fig. 6. Nanostructures of GSH products. SEM images of (a) one-stage GSHs on LDO flakes and (b) two-stage GSHs on LDO flakes. TEM images of (c) one-stage GSHs on LDO flakes, (d) purified one-stage GSHs, (e) two-stage GSHs on LDO flakes and (f) purified two-stage GSHs, (g) high resolution TEM image of the few-layer graphene domain of two-stage GSHs.

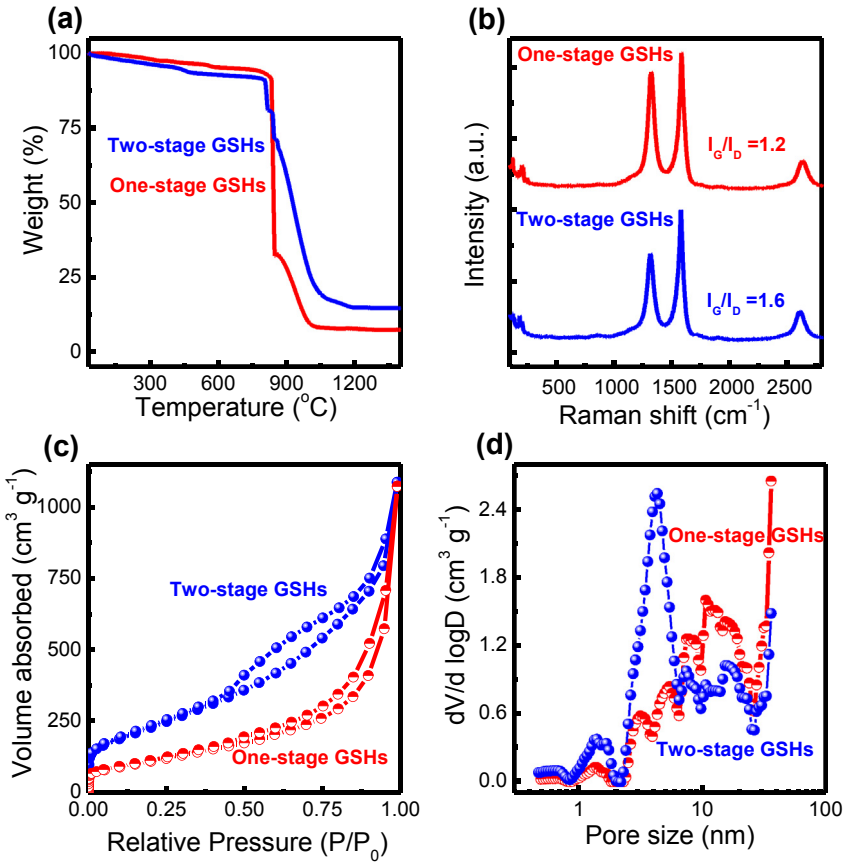

Fig. 7. Characterization of GSH products grown in routine fluidized bed reactor and coupled reactor. (a) TGA profiles under CO_2 atmosphere, (b) Raman spectra, (c) N_2 adsorption–desorption isotherms, and (d) pore size distributions. (A colour version of this figure can be viewed online.)

graphitization. The position of 2D peaks was also reduced from 2635 cm^{-1} for one-stage GSHs to 2608 cm^{-1} for two-stage GSHs, indicating the significant increase of the amount of single-walled CNTs and single-layered graphene in the GSHs. In addition, the SSA of two-stage GSHs calculated by the multipoint BET method from the N_2 adsorption/desorption isotherms (Fig. 7c) was increased to 833.2 from 401.5 $m^2\ g^{-1}$ for one-stage GSHs, along with the improvement of the total pore volume of the hybrids from 1.2 to 1.4 $cm^3\ g^{-1}$. As shown in Fig. 7d, these two samples displayed very different pore size distributions, the two-stage GSHs possessed more micropores at around 1.5 nm and mesopores at about 4.5 nm, while the predominant pores for one-stage GSHs was around 11.6 nm. This was attributed from a high ratio of amorphous carbon during the continuous growth of GSHs in the one-stage method.

The summary of the comparison of the characteristics of the two-stage GSHs and one-stage GSHs was listed in Table 1. The properties of two-stage GSHs were significantly advantageous over the one-stage GSHs in almost all aspects. The quality of as-produced GSHs was greatly enhanced using the proposed two-stage growth strategy, which paved the way for the bulk controllable production of high quality GSHs in a more efficient way.

4. Conclusions

In-situ characterization of the catalytic growth of GSHs on bifunctional FeMgAl LDO catalysts was conducted in a TG reactor. Both the amount and the rate of mass variation were *in-situ* recorded in a quantitative way. The growth of single-walled CNTs and graphene were clearly distinguished in the growth duration. Combined with the results collected by the online mass spectroscopy and TEM, it was found that the CNTs were grown with a relatively rapid rate in the first stage, while graphene were deposited in a slow rate during the whole growth process on LDO catalysts. With the guidance of the *in-situ* characterization, a two-stage growth was proposed to enhance the process efficiency and

Table 1
A summary of the GSH products grown with the proposed two-stage method and the routine one-stage method.

Sample	Two-stage GSHs	One-stage GSHs
Weight loss in Region I (790 °C–870 °C)	34.7%	70.8%
Weight loss in Region II (870 °C–1100 °C)	65.3%	29.2%
SSA ($m^2\ g^{-1}$)	833.2	401.5
Pore volume ($cm^3\ g^{-1}$)	1.4	1.2
I_G/I_D in Raman spectra	1.6	1.2
The position of 2D peaks in Raman spectra (cm^{-1})	2608	2635
Conductivity (S cm^{-1})	16.3	13.3

product quality for bulk production of GSHs, in which a high feed rate of carbon source was employed in the first 90 s, while a low feed rate was applied in the second-stage growth. Therefore, the I_G/I_D ratio was increased from 1.2 for one-stage GSHs to 1.6 for two-stage GSHs, and the specific surface area of two-stage GSHs increased to 833.2 from 401.5 $m^2\ g^{-1}$ for one-stage GSHs, along with the improvement of the total pore volume of the hybrids from 1.2 to 1.4 $cm^3\ g^{-1}$. During the two-stage growth of GSHs, the deposition of amorphous carbon byproducts was greatly suppressed, and the quality of the GSH products was significantly improved. This work provided a general concept to rationally design the reactor based on the unique kinetic behavior probed by the *in-situ* characterization, which can be applied for other materials and chemical production.

Acknowledgments

This work was supported by the Natural Scientific Foundation of China (21306102 and 21422604), Tsinghua University Initiative Scientific Research Program (2014z22076), and the National Basic Research Program of China (2011CB932602 and 2015CB932500).

References

[1] M.F.L. De Volder, S.H. Tawfick, R.H. Baughman, A.J. Hart, Carbon nanotubes: present and future commercial applications, Science 339 (2013) 535–539.
[2] Q. Zhang, J.Q. Huang, W.Z. Qian, Y.Y. Zhang, F. Wei, The road for nanomaterials industry: a review of carbon nanotube production, post-treatment, and bulk applications for composites and energy storage, Small 9 (2013) 1237–1265.
[3] W. Wang, S.R. Guo, M. Penchev, I. Ruiz, K.N. Bozhilov, D. Yan, et al., Three dimensional few layer graphene and carbon nanotube foam architectures for high fidelity supercapacitors, Nano Energy 2 (2013) 294–303.
[4] G.L. Tian, M.Q. Zhao, D.S. Yu, X.Y. Kong, J.Q. Huang, Q. Zhang, et al., Nitrogen-doped graphene/carbon nanotube hybrids: in situ formation on bifunctional catalysts and their superior electrocatalytic activity for oxygen evolution/reduction reaction, Small 10 (2014) 2251–2259.
[5] L.L. Zhang, Z.G. Xiong, X.S. Zhao, Pillaring chemically exfoliated graphene oxide with carbon nanotubes for photocatalytic degradation of dyes under visible light irradiation, ACS Nano 4 (2010) 7030–7036.
[6] M.Q. Zhao, X.F. Liu, Q. Zhang, G.L. Tian, J.Q. Huang, W.C. Zhu, et al., Graphene/single-walled carbon nanotube hybrids: one-step catalytic growth and applications for high-rate Li-S batteries, ACS Nano 6 (2012) 10759–10769.
[7] W. Wang, I. Ruiz, S. Guo, Z. Favors, H.H. Bay, M. Ozkan, et al., Hybrid carbon nanotube and graphene nanostructures for lithium ion battery anodes, Nano Energy 3 (2014) 113–118.
[8] Y. Wu, T. Zhang, F. Zhang, Y. Wang, Y. Ma, Y. Huang, et al., *In situ* synthesis of graphene/single-walled carbon nanotube hybrid material by arc-discharge and its application in supercapacitors, Nano Energy 1 (2012) 820–827.
[9] D. Yu, K. Goh, H. Wang, L. Wei, W. Jiang, Q. Zhang, et al., Scalable synthesis of hierarchically structured carbon nanotube-graphene fibres for capacitive energy storage, Nat. Nanotechnol. 9 (2014) 555–562.
[10] L. Jiang, L. Sheng, C. Long, Z. Fan, Densely packed graphene nanomesh-carbon nanotube hybrid film for ultra-high volumetric performance supercapacitors, Nano Energy 11 (2015) 471–480.
[11] M. Sun, G. Wang, C. Yang, H. Jiang, C. Li, A graphene/carbon nanotube@π;-conjugated polymer nanocomposite for high-performance organic supercapacitor electrodes, J. Mater. Chem. A 3 (2015) 3880–3890.
[12] V.C. Tung, L.M. Chen, M.J. Allen, J.K. Wassei, K. Nelson, R.B. Kaner, et al., Low-temperature solution processing of graphene-carbon nanotube hybrid materials for high-performance transparent conductors, Nano Lett. 9 (2009) 1949–1955.
[13] S.S. Li, Y.H. Luo, W. Lv, W.J. Yu, S.D. Wu, P.X. Hou, et al., Vertically aligned carbon nanotubes grown on graphene paper as electrodes in lithium-ion batteries and dye-sensitized solar cells, Adv. Energy Mater. 1 (2011) 486–490.
[14] B. Li, X.H. Cao, H.G. Ong, J.W. Cheah, X.Z. Zhou, Z.Y. Yin, et al., All-carbon electronic devices fabricated by directly grown single-walled carbon nanotubes on reduced graphene oxide electrodes, Adv. Mater. 22 (2010) 3058–3061.
[15] X.C. Dong, J. Chen, Y.W. Ma, J. Wang, M.B. Chan-Park, X.M. Liu, et al., Super-hydrophobic and superoleophilic hybrid foam of graphene and carbon nanotube for selective removal of oils or organic solvents from the surface of water, Chem. Commun. 48 (2012) 10660–10662.
[16] Y.G. Li, W. Zhou, H.L. Wang, L.M. Xie, Y.Y. Liang, F. Wei, et al., An oxygen reduction electrocatalyst based on carbon nanotube-graphene complexes, Nat. Nanotechnol. 7 (2012) 394–400.
[17] R. Lv, E. Cruz-Silva, M. Terrones, Building complex hybrid carbon architectures by covalent interconnections: graphene–nanotube hybrids and more, ACS Nano 8 (2014) 4061–4069.
[18] D.Y. Cai, M. Song, C.X. Xu, Highly conductive carbon-nanotube/graphite-oxide hybrid films, Adv. Mater. 20 (2008) 1706–1709.
[19] L. Sun, W. Kong, Y. Jiang, H. Wu, K. Jiang, J. Wang, et al., Super-aligned carbon nanotube/graphene hybrid materials as a framework for sulfur cathodes in high performance lithium sulfur batteries, J. Mater. Chem. A 3 (2015) 5305–5312.
[20] F. Tristán-López, A. Morelos-Gómez, S.M. Vega-Díaz, M.L. García-Betancourt, N. Perea-López, A.L. Elías, et al., Large area films of alternating graphene–carbon nanotube layers processed in water, ACS Nano 7 (2013) 10788–10798.
[21] H.R. Byon, S.W. Lee, S. Chen, P.T. Hammond, Y. Shao-Horn, Thin films of carbon nanotubes and chemically reduced graphenes for electrochemical micro-capacitors, Carbon 49 (2011) 457–467.
[22] T.K. Hong, D.W. Lee, H.J. Choi, H.S. Shin, B.S. Kim, Transparent, flexible conducting hybrid multi layer thin films of multiwalled carbon nanotubes with graphene nanosheets, ACS Nano 4 (2010) 3861–3868.
[23] D.T. Pham, T.H. Lee, D.H. Luong, F. Yao, A. Ghosh, V.T. Le, et al., Carbon nanotube-bridged graphene 3D building blocks for ultrafast compact supercapacitors, ACS Nano 9 (2015) 2018–2027.
[24] J.J. Shao, W. Lv, Q.G. Guo, C. Zhang, Q. Xu, Q.H. Yang, et al., Hybridization of graphene oxide and carbon nanotubes at the liquid/air interface, Chem. Commun. 48 (2012) 3706–3708.
[25] Y. Wang, Y.P. Wu, Y. Huang, F. Zhang, X. Yang, Y.F. Ma, et al., Preventing graphene sheets from restacking for high-capacitance performance, J. Phys. Chem. C 115 (2011) 23192–23197.
[26] S.B. Bon, L. Valentini, J.M. Kenny, L. Peponi, R. Verdejo, M.A. Lopez-Manchado, Electrodeposition of transparent and conducting graphene/carbon nanotube thin films, Phys. Status Solidi A 207 (2010) 2461–2466.
[27] Z.J. Fan, J. Yan, L.J. Zhi, Q. Zhang, T. Wei, J. Feng, et al., A three-dimensional carbon nanotube/graphene sandwich and its application as electrode in supercapacitors, Adv. Mater. 22 (2010) 3723–3728.
[28] S.Q. Chen, P. Chen, Y. Wang, Carbon nanotubes grown *in situ* on graphene nanosheets as superior anodes for Li-ion batteries, Nanoscale 3 (2011) 4323–4329.
[29] F. Du, D.S. Yu, L.M. Dai, S. Ganguli, V. Varshney, A.K. Roy, Preparation of tunable 3D pillared carbon nanotube-graphene networks for high-performance capacitance, Chem. Mater. 23 (2011) 4810–4816.
[30] Y. Zhu, L. Li, C. Zhang, G. Casillas, Z. Sun, Z. Yan, et al., A seamless three-dimensional carbon nanotube graphene hybrid material, Nat. Commun. 3 (2012) 1225.
[31] C. Tang, Q. Zhang, M.-Q. Zhao, J.-Q. Huang, X.-B. Cheng, G.-L. Tian, et al., Nitrogen-doped aligned carbon nanotube/graphene sandwiches: facile catalytic growth on bifunctional natural catalysts and their applications as scaffolds for high-rate lithium-sulfur batteries, Adv. Mater. 26 (2014) 6100–6105.
[32] R.K. Paul, M. Ghazinejad, M. Penchev, J.A. Lin, M. Ozkan, C.S. Ozkan, Synthesis of a pillared graphene nanostructure: a counterpart of three-dimensional carbon architectures, Small 6 (2010) 2309–2313.
[33] C. Tang, Q. Zhang, M.-Q. Zhao, G.-L. Tian, F. Wei, Resilient aligned carbon nanotube/graphene sandwiches for robust mechanical energy storage, Nano Energy 7 (2014) 161–169.
[34] T. Odedairo, J. Ma, Y. Gu, J. Chen, X.S. Zhao, Z. Zhu, One-pot synthesis of carbon nanotube-graphene hybrids *via* syngas production, J. Mater. Chem. A 2 (2014) 1418–1428.
[35] C.M. Li, M. Wei, D.G. Evans, X. Duan, Layered double hydroxide-based nanomaterials as highly efficient catalysts and adsorbents, Small 10 (2014) 4469–4486.
[36] G.-L. Tian, Q. Zhang, M.-Q. Zhao, H.-F. Wang, C.-M. Chen, F. Wei, Fluidized-bed cvd of unstacked double-layer templated graphene and its application in supercapacitors, AIChE J. 61 (2015) 747–755.
[37] G.L. Tian, M.Q. Zhao, B.S. Zhang, Q. Zhang, W. Zhang, J.Q. Huang, et al., Monodisperse embedded nanoparticles derived from an atomic metal-dispersed precursor of layered double hydroxide for architectured carbon nanotube formation, J. Mater. Chem. A 2 (2014) 1686–1696.
[38] Z.J. Hu, K.J. Hüttinger, Influence of the surface area/volume ratio on the chemistry of carbon deposition from methane, Carbon 41 (2003) 1501–1508.
[39] D.A. Gomez-Gualdron, P.B. Balbuena, Effect of metal cluster-cap interactions on the catalyzed growth of single-wall carbon nanotubes, J. Phys. Chem. C 113 (2009) 698–709.
[40] R. Rao, N. Pierce, D. Liptak, D. Hooper, G. Sargent, S.L. Semiatin, et al., Revealing the impact of catalyst phase transition on carbon nanotube growth by in situ raman spectroscopy, ACS Nano 7 (2013) 1100–1107.
[41] M. Liu, R. Xiang, W. Cao, H.Q. Zeng, Y.Q. Su, X.C. Gui, et al., Is it possible to enhance raman scattering of single-walled carbon nanotubes by metal particles during chemical vapor deposition? Carbon 80 (2014) 311–317.
[42] K. Reinhold-Lopez, A. Braeuer, B. Romann, N. Popovska-Leipertz, A. Leipertz, Simultaneous *in situ* raman monitoring of the solid and gas phases during the formation and growth of carbon nanostructures inside a cold wall CCVD reactor, Carbon 78 (2014) 164–180.
[43] Z.-J. Wang, G. Weinberg, Q. Zhang, T. Lunkenbein, A. Klein-Hoffmann, M. Kurnatowska, et al., Direct observation of graphene growth and associated copper substrate dynamics by *in situ* scanning electron microscopy, ACS Nano 9 (2015) 1506–1519.
[44] A.M. Beese, D. Papkov, S.Y. Li, Y. Dzenis, H.D. Espinosa, *In situ* transmission electron microscope tensile testing reveals structure-property relationships in carbon nanofibers, Carbon 60 (2013) 246–253.

[45] A. Rinaldi, J.P. Tessonnier, M.E. Schuster, R. Blume, F. Girgsdies, Q. Zhang, et al., Dissolved carbon controls the initial stages of nanocarbon growth, Angew. Chem. Int. Ed. 50 (2011) 3313–3317.
[46] Y.J. Tian, Z. Hu, Y. Yang, X.Z. Wang, X. Chen, H. Xu, et al., *In situ* TA-MS study of the six-membered-ring-based growth of carbon nanotubes with benzene precursor, J. Am. Chem. Soc. 126 (2004) 1180–1183.
[47] T.C. Chen, M.Q. Zhao, Q. Zhang, G.L. Tian, J.Q. Huang, F. Wei, *In situ* monitoring the role of working metal catalyst nanoparticles for ultrahigh purity single-walled carbon nanotubes, Adv. Funct. Mater. 23 (2013) 5066–5073.
[48] K.J. MacKenzie, O.M. Dunens, A.T. Harris, Insights into carbon nanotube growth using an automated gravimetric apparatus, Carbon 59 (2013) 344–365.
[49] R. Philippe, P. Serp, P. Kalck, S. Bordere, D. Plee, P. Gaillard, et al., Kinetic modeling study of carbon nanotubes synthesis by fluidized bed chemical vapor deposition, AIChE J. 55 (2009) 465–474.
[50] F. Danafar, A. Fakhru'l-Razi, M.A.M. Salleh, D.R.A. Biak, Fluidized bed catalytic chemical vapor deposition synthesis of carbon nanotubes–a review, Chem. Eng. J. 155 (2009) 37–48.
[51] Q. Zhang, J.Q. Huang, M.Q. Zhao, W.Z. Qian, F. Wei, Carbon nanotube mass production: principles and processes, ChemSusChem 4 (2011) 864–889.
[52] C.H. See, A.T. Harris, A review of carbon nanotube synthesis *via* fluidized-bed chemical vapor deposition, Ind. Eng. Chem. Res. 46 (2007) 997–1012.
[53] A.F. Cunha, J.J.M. Orfao, J.L. Figueiredo, Methane decomposition on Ni–Cu alloyed raney-type catalysts, Int. J. Hydrogen Energy 34 (2009) 4763–4772.
[54] Y. Li, X.B. Zhang, L.H. Shen, J.H. Luo, X.Y. Tao, F. Liu, et al., Controlling the diameters in large-scale synthesis of single-walled carbon nanotubes by catalytic decomposition of CH_4, Chem. Phys. Lett. 398 (2004) 276–282.
[55] M.Q. Zhao, Q. Zhang, J.Q. Huang, J.Q. Nie, F. Wei, Layered double hydroxides as catalysts for the efficient growth of high quality single-walled carbon nanotubes in a fluidized bed reactor, Carbon 48 (2010) 3260–3270.
[56] Q. Zhang, M.Q. Zhao, J.Q. Huang, Y. Liu, Y. Wang, W.Z. Qian, et al., Vertically aligned carbon nanotube arrays grown on a lamellar catalyst by fluidized bed catalytic chemical vapor deposition, Carbon 47 (2009) 2600–2610.
[57] Q. Zhang, M.Q. Zhao, J.Q. Huang, J.Q. Nie, F. Wei, Mass production of aligned carbon nanotube arrays by fluidized bed catalytic chemical vapor deposition, Carbon 48 (2010) 1196–1209.
[58] D.Y. Kim, H. Sugime, K. Hasegawa, T. Osawa, S. Noda, Sub-millimeter-long carbon nanotubes repeatedly grown on and separated from ceramic beads in a single fluidized bed reactor, Carbon 49 (2011) 1972–1979.
[59] Z.M. Chen, D.Y. Kim, K. Hasegawa, T. Osawa, S. Noda, Over 99.6 wt%-pure, sub-millimeter-long carbon nanotubes realized by fluidized-bed with careful control of the catalyst and carbon feeds, Carbon 80 (2014) 339–350.
[60] M.Q. Zhao, H.J. Peng, Q. Zhang, J.Q. Huang, G.L. Tian, C. Tang, et al., Controllable bulk growth of few-layer graphene/single-walled carbon nanotube hybrids containing Fe@C nanoparticles in a fluidized bed reactor, Carbon 67 (2014) 554–563.
[61] N. Matsumoto, G. Chen, M. Yumura, D.N. Futaba, K. Hata, Quantitative assessment on the importance of purity on the properties of single wall carbon nanotubes, Nanoscale 7 (2015) 5126–5133.